Resumen

El comportamiento de daño por contacto de dos grados de carburos cementados, tipo WC-Co con diferentes microestructuras, fue estudiado. El daño por contacto fue inducido por indentadores esféricos siguiendo los métodos del contacto hertziano y ensayo de rayado. En el ensayo hertziano cuatro diferentes indentadores fueron utilizados: dos indentadores de metal duro del tipo WC-Ni que tenían diámetros de 3.2 milímetros y 5 milímetros, un indentador de alúmina y un de zafiro con diámetros de 3.2 milímetros. Los indentadores de alúmina y de zafiro se rompieron en las cargas relativamente bajas y la evaluación del daño fue realizada principalmente estudiando el daño inducido por los indentadores de WC-Ni. En el ensayo de rayado un indentador de diamante de Rockwell, teniendo radio 0.2 milímetro, fue utilizado. Este ensayo fue hecho con la carga constante y con el modo progresivo. Las pruebas de barra y los especimenes consolidados fueron utilizados en estos dos ensayos. Los ensayos hechos en las pruebas de barra sirvieron para calcular la deformación y los ensayos hechos en especimenes consolidados fueron utilizadas estudiar el daño subsuperficie. En estos dos ensayos las pruebas de grado más dulce demostraron ser más dúctiles que las de más duro, no demostrando ningunas grietas. En este último, aunque demostró una cierta ductilidad, las grietas eran evidentes, pero solamente en las cargas intermedias y altas.

Abstract

The contact damage behaviour of two cemented carbide grades, type WC-Co, with different microstructures were studied. The contact damage were induced by spherical indenters following the Hertzian contact and scratch test procedure. In Hertzian contact test four different indenters were used: two hardmetal indenters of type WC-Ni having diameters 3.2 mm and 5 mm, one of alumina and one of sapphire both with diameter 3.2 mm. The alumina and sapphire indenters broke at relatively low loads and the evaluation of the contact damage was mainly carried out studying the damage induced by WC-Ni indenters. In scratch test a Rockwell diamond indenter, having radius 0.2 mm, was used. This test was made both with constant load and progressive mode. In these tests both bar and bonded specimens were used. The indentation and scratch tests provided information for evaluating deformation and those made in bonded specimens were used to study the subsurface damage. In both tests the softer grade proved to be more ductile than the harder one, not showing any cracks. For the latter, although even it showed some ductility, the cracks were evident, but only at intermediate and high loads.

Table of contents

1. Introduction

In many areas of engineering, demands for higher functionality and reliability are leading to the increasing use of materials with specially tailored properties. Examples of these properties include wear resistance, high heat resistance, increased mechanical strength, toughness and low specific gravity.

Cemented carbides belong to a class of hard, wear-resistant, refractory materials in which the hard carbide particles are bound together, or cemented, by a soft and ductile metal binder. Tungsten carbide (WC) is the main metallic hard material used and cobalt (Co) is the main binder. Cemented carbides were first developed in the early 1920s and cobalt was soon found to be the best bonding material. This was due to various properties of cobalt, among them is the high melting point (1495 $^{\circ}$C), which makes it a good refractory metal. The tungsten carbide phase contributes to hardness, stiffness, mechanical resistance and wear resistance of cemented carbides, whereas the metallic phase, cobalt, contributes to toughness and improves machinability.

Over the years, the basic tungsten carbide-cobalt (WC-Co) material has been modified to produce a variety of cemented carbides, which are used in a wide range of applications, including metal cutting, mining, construction, rock drilling, metal forming, structural components, and wear parts [1]. Common to all these applications is the fact that cemented carbides are exposed to contact loading conditions against other materials. Such a damage, in the scientific literature referred to a “indentation damage” bears profoundly on a wide range of other mechanical properties (strength, toughness and wear, among others) seriously compromising the useful lifetime of hardmetal tools and components [2]. In the present investigation, contact damage on cemented carbides is addressed by studying their Hertzian contact behaviour with spherical indenters. In doing so, special attention is paid to document damage mechanisms resulting from simple indentation and sliding contact loading conditions on hardmetals with different microstructures.

2. Damage behaviour of brittle materials

As it was described in the previous section, this work deals with contact damage, induced on hardmetals by indenters, as a function of microstructure. This is experimentally carried out by means of Hertzian contact and scratch tests. Hertzian contact test is a method extensively used in the analysis and characterisation of fracture and deformation properties of brittle materials. Although in many conventional tests cemented carbides, as well as most engineering ceramics, behave in an almost completely brittle manner, this may not be the case under spherical contact loading. In a Hertzian contact test a spherical indenter is applied by certain load in a flat and polished specimen surface, inducing a damage, that can be either cone cracking, for brittle solids, called Hertzian cone crack or a subsurface quasi-plastic deformation, for tougher solids, or something in between. The schema for Hertzian contact test is shown in figure 2.1.

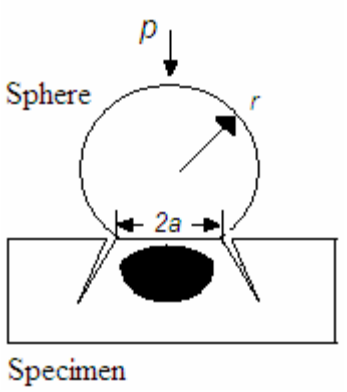

Figure 2.1. Hertzian contact test.

For brittle solids the damage begins as a surface ring crack, figure 2.2, and propagates downward in fixed angle which is dependent on the Poisson's ratio of the brittle material [3]. This angle is usually between 20˚ and 30˚ from the surface. When there are multiple surface cracks as in figure 2.2, the expanding contact circle engulfs the first surface ring and a second ring crack is formed, but after unloading the crack usually remains visible due to imperfect closure at the crack interface [2]. If the material is tougher there will be instead a quasi-plastic deformation beneath the surface, as marked with black in figure 2.1. This is due to compressive shear stresses, which have their maximum along the contact axis at a depth ≈

0.5a below the surface [2]. The principal compression stresses in the Hertzian field are $-a_1$ and $-a_3$, which usually are unequal [4] and consequently there is a component of shear acting on planes inclined to the principal axes. The shear component initiates intragranular faults, which arrest at the grain boundaries and intensify stress there. If such local stress intensity factor exceeds a critical level, there will be micro-cracks [4], figure 2.3. This compression field will also suppress cone cracking mechanisms [2,4].

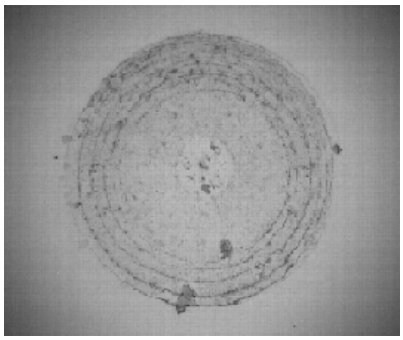

Figure 2.2. A series of wholly developed surface ring cracks in hardmetal grade 10F, Load applied with a WC-Ni indenter of diameter 3.2 mm.

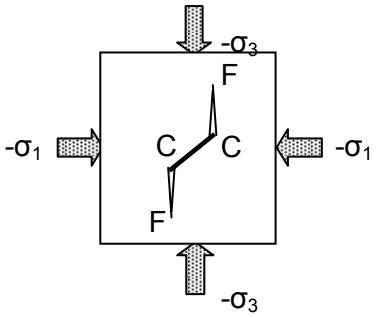

Figure 2.3. Schema for shear-fault/wing crack system.

In scratch testing a conical indenter is used by applying either a constant or incremental load at the specimen surface while it is moved with constant speed. A large number of information might be obtained from this test. For example, curves for the penetration depth, residual penetration depth, frictional normal and tangential forces, and acoustic emission are delivered. The depth penetrated by the indenter depends of the hardness of the material tested and as the indenter has conical form, the width of the scratch path depends also of this parameter. This fact yields the possibility of calculating the sliding stress-strain and deformation-load curves, which will be presented later in this report.

3.Experimental procedure

Two different hardmetal grades were examined: 10F and 16M. The basic microstructural characteristics of both materials are shown in table 3.1.

Parameter	10F	16M
V_{Co} (%)	$10{,}20 \pm 0{,}01$	$16{,}37 \pm 0{,}02$
d_{WC} (mm)	0,39	1,06

Table 3.1. Material parameters for grades used. V_{Co} is volume of cobalt and d_{WC} is the size of tungsten carbide grain.

The Vickers hardness (HV30) of these two grades are $19{,}23 \pm 3{,}7$ GPa for 10M and $15{,}4 \pm 2{,}5$ GPa for 16M, data taken from [5].

3.1 Hertzian contact test

3.1.1 Indentation of bar specimens

Bar specimens with dimensions 25 mm*4 mm*3 mm, corresponding to each hardmetal grade 10F and 16M, were used. One of the largest surfaces was optically polished following a 3-step procedure. First, the surface was ground during 5 minutes to 68 mm grade finish using a diamond disc in a Buehler polishing machine Thereafter the grounded face was polished during 5 minutes to 30 mm grade finish using a diamond paste applied on a wood disc. The final step consisted of polishing the specimens, again with diamond paste on a wood disc, during 15 minutes to 6 mm grade finish, The two polishing steps were realized in a Kent 3 polishing machine. In all three steps the lubrication used was water. These specimens were employed for indentation stress-strain measurements and the polished surfaces were gold coated prior to indentation.

Indentations were made in an Instron testing machine, model 8511. Following a pre-load of 50 N, load was increased at a constant rate of 50N/ s until desired value was achieved. Then it was held during 10 seconds before decreasing to the start preload value at similar load decreasing rate. The remaining 50 N was removed manually. A series of indentations was performed on each specimen up to the following P_{app} values: 100 N, 200 N, 300 N, 400 N, 500 N, 600 N, 700 N, 800 N, 900 N, 1000 N, 2000 N, 3000 N, 4000 N, 5000 N, 6000 N and 7000 N. These tests were conducted with different indenters: hardmetal (WC-Ni) spheres of diameters 3.2 and 5.0 mm, alumina sphere of diameter 3.2 mm and a sapphire sphere of diameter 3.2 mm.

Only the 5.0 mm WC-Ni sphere endured the load of 7000 N for both studied materials. The other spheres broke at lower loads, possibly due to their intrinsic hard-brittle character. Additionally, whereas the 3.2 mm WC-Ni sphere sustained the load of 7000 N when the indentation was made on the softer material, that is 16M, it broke too for applied load of 6000 N in the harder material, 10F. The 3.2 mm sphere of alumina broke by the load of 1800 N when indenting 10F and by the load of 2780 for 16M, whereas the 3.2 mm sphere of sapphire did not sustain loads of 800 N and 630 N for 16M and 10F, respectively. After indentations were made the specimens were examined in optical and scanning electron microscopy (SEM).

Fracture toughness (K_{IC}) and rupture indentation loads (N) for indenters are shown in table 3.2.

$D_{indenter}$ = 3,2 mm		$P_{rupture\ indenter}$ (N)	
Indenter	$K_{IC\ indenter}$ (MPa√m)	10F	16M
Sapphire	2,0	630	800
Alumina	3,4	1800	2780
WC-Ni	11,1	6000	7000

Table 3.2. Fracture toughness (K_{IC}) and rupture indentation loads (N) for indenters used in tests. The value for alumina is an average taken from ASM Metal Handbook, Vol. 2, 10th edition. The sapphire value comes from web page: http:/www.ceramics.nist.gov/srd/ summary/ftgsaph.htm (Visited 10th of January 2005) and the WC-Ni value is approximated from similar materials.

The contact radius *a* for each indentation was measured from the residual impression left in the gold coated surface to enable calculation of the contact pressure,

$$p_o = \frac{P}{\pi a^2}, \qquad \textbf{Eq. 3.1}$$

as well as the indentation strain,

$$\frac{a}{r}, \qquad \textbf{Eq. 3.2}$$

The indentation stress-strain curve was thereafter plotted.

3.1.2 Indentation of bonded specimens

A different set of specimens were cut in the middle in order to make it possible to study the indentation effects on the cross sections. In this case, the cut specimens were embedded in bakelite and one face of the specimens was grounded and polished almost in the same manner as in the case of bar specimens to 6 mm grade finish. Here the diamond paste and the wood disc were replaced by a diamond suspension and polishing cloth, with special lubrication. After this was done the bakelite was broken and the two pieces were tightly bonded with Locktite® super clue-3® with their polished surfaces facing each other. The joined pieces were embedded in bakelite again and the joint surface was polished following the same procedure as above described, to 6 mm grade finish. Figure 3.2 shows the different steps for polishing the bonded pieces.

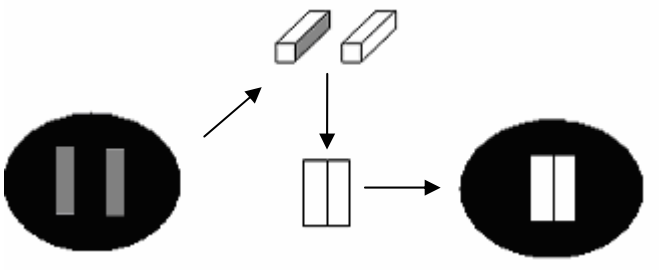

Figure 3.2*a* Figure 3.2*b* Figure 3.2*c*

Figure 3.2. *a*) Two pieces were embedded in bakelite in order to be able to polish them as plane as possible. *b*) After the polishing the bakelite was broken and the pieces were clued together with polished sides facing each other, *c*) Finally the bonded pieces were polished to 6-mm grade finish.

The indentations were made using the same Instron testing machine as earlier. The indentations were attempted, as precise as it was possible, at the polished joint of the two pieces, figure 3.3. Immediately after the indentations were made, the specimens' surfaces were examined by means of optical microscopy. Similar study was performed on the cross-sections after breaking the bakelite and when bonded pieces were separated and cleaned by using acetone. The cross-sections were also examined in SEM.

For these indentations it was decided to use the WC-Ni sphere of 3.2 mm, as the spheres of alumina and sapphire broke at relatively low loads in earlier test. The loads used here, same for both grades, were 300 N, 400 N, 500 N, 600 N, 700 N, 800 N, 900 N, 1000 N, 2000 N and 3000 N.

The purpose was to find out the critical load where the damage appeared for the first time besides evaluating how the damage was developed as the load was increased. These "critical" loads were chosen after examining the indentation stress-strain curves. As long as there is only elastic deformation, the points in this curve form a straight line through zero [2]. However, when the material response is irreversible, i.e. when there is quasi-plastic deformation, more or less pronounced divergence from this linear behaviour takes place, depending of the degree of quasi-plastic deformation. The indentations were made in the same manner as in the previous test, that is, the load increasing and decreasing rate was 50 N/s with a pre-load of 50 N. Additionally, when the desired maximum load for each indentation was achieved, it was held constant during ten seconds.

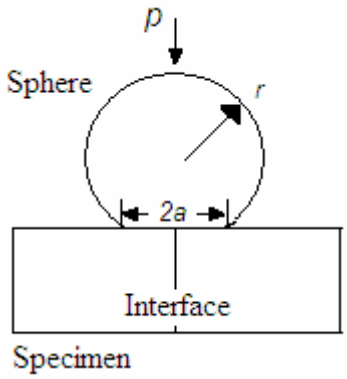

Figure 3.3. Hertzian test geometry for bonded-interface specimen.

3.2 Scratch test

The scratch test was carried out by using both the bar specimens and the bonded cut specimens embedded in bakelite. The bar specimens were used to compare the deformations with those obtained from Hertzian contact test and to find out the critical loads for damage, for

subsequent use in testing the bonded pieces. The bonded specimens were employed to be able of studying cross sections, as in the indentation test. The scratching was made in a CSM® instrument revetest® machine and the indenter used was a Rockwell diamond indenter with radius 0.2 mm, serial number Q-239.

Two tests with different sliding distances were made on the bar specimens, 2 mm and 10 mm. In these tests the load was increased constantly at a rate of 120N/ minute, while the sliding speed was held constant. The scratch distance for the first test was 2 mm and the maximum loads used were 150 N for 10F and 100 N for 16M. The decision to use these loads was taken after examination the scratch trace from a pre-test, where it was observed that it was unnecessary to use higher loads than those named above. This was because the damage character did not seem to vary after these loads, although its magnitude increased, as expected.

The deformation was measured in about 20 different points along the scratch path and the indentation stress-strain curves were plotted. For calculations of the contact pressure and strain, the same equations were used as in the indentation test, namely equation 3.1 for the contact pressure and equation 3.2 for the strain. In these equations a was replaced by $w/2$, that is, by half width of the scratch trace. The specimens were also examined in optical microscopy to discern what loads should be used for constant-load scratching in the bonded pieces. Attention was drawn to points were it seemed to have occurred something, for example the load at which the cracks began to appear in 10F. (in 16M no cracks were detected) or the load at which the material began to chip off in the borders of the scratch trace. To determine critical loads the acoustic emission curve was also used.

To find out if the indenter's sliding speed had an influence on deformation response, a comparative test with scratch distance of 10 mm was made while the load rate was still 120N/ min, and consequently the sliding speed was higher. The curves for the 10 mm scratch distance as well as for constant load test are included in stress-strain diagrams.

In scratching the bonded pieces the indenter was moved perpendicular to the artificial joint, figure 3.4, and the load was held constant. The loads used are shown in table 3.3. Each scratch trace was examined in optical microscopy, and the width of the path was measured

immediately after the scratching was made. Later on the bakelite was broken, pieces were separated and cleaned using acetone, and the cross sections were studied and photographed.

Grade	Load (N)											
10 F	10	15	20	25	30	35	40	50	60	70	90	110
16 M	10	15	20	25	30	35	40	45	50	75	90	

Table 3.3. The loads used in indenting the bonded specimens.

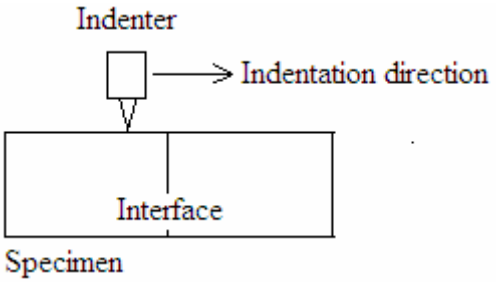

Figure 3.4. Scratching of bonded specimen

4. Results and Discussion

4.1 Indentation test

Indentation stress-strain curves for specimens used in Hertzian contact test were plotted from measurements of contact radius *a* left in the gold coating at each given load *P* and sphere radius *r*. Figures 4.1*a* and *b* show two examples of prints left in the gold coating.

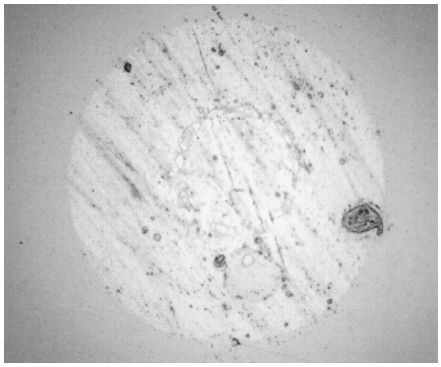

Figure 4.1*a*.

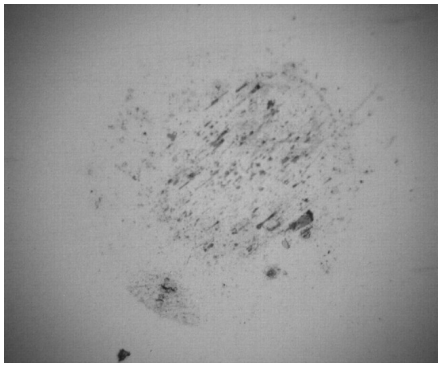

Figure 4.1*b*

Figure 4.1. Indentation in figure 4.1*a* corresponds to 16M using a sapphire sphere of diameter 3.2 mm and with load 500 N. Indentation in figure 4.1*b* is made by WC-Ni indenter, diameter 5 mm and load 2000 N in the same material.

Data representing indentation stress,

$$p_o = \frac{P}{\pi a^2}, \qquad \textbf{Eq. 3.1}$$

as a function of indentation strain,

$$\frac{a}{r}, \qquad \textbf{Eq. 3.2}$$

are plotted in figures 4.2*a*, *b*, *c* and *d*.

4.1.1 Indentation of 10F

The inclined solid lines through the origin are the linear relations for purely elastic contacts from Hertzian theory [2]

$$p_o = \frac{3E}{4\pi k} \times \frac{a}{r} \qquad \textbf{Eq. 4.1}$$

where E is Young's modulus of the indented material and

$$k = \frac{9}{16}\left[\left(1-\upsilon^2\right)+\left(1-\upsilon'^2\right)\frac{E}{E'}\right] \qquad \textbf{Eq. 4.2}$$

is a dimensionless coefficient, with υ Poisson's ratio and the prime notation denoting the indenter material. The theoretic values of slopes,

$$\frac{3E}{4\pi k}, \qquad \textbf{Eq. 4.3}$$

for 10F, with E= 593 GPa and υ= 0.21, are shown in table 4.1.

Indenter	*E'* (GPa)	υ	**Slope (GPa)**
WC-Ni	500	0,21	**120,44**
Alumina	390	0,26	**106,03**
Sapphire	345	0,24- 0,30	**98,37**

Table 4.1. The theoretic slope for indenters used in tests.

The alumina data is taken from Ceramic Oxide Fabricators, http://www.cof.com.au/AluminaData.shtml, visited 10th January 2005.

Sapphire data comes from Guild Optical Associates, inc. http://www.guildoptics.com/properties.html, visited 10th januari 2005.

The corresponding experimental values calculated from curves in figures 4.2*a*, *b*, *c* and *d* for 10F are shown in table 4.2.

Indenter	**Slope (GPa)**
WC-Ni Sphere 3.2 mm	**90,52**
WC-Ni Sphere 5 mm	**96,34**
Alumina	**95,74**
Sapphire	**91,40**

Table 4.2. Experimental values of slopes for different indenters from the curves for 10F.

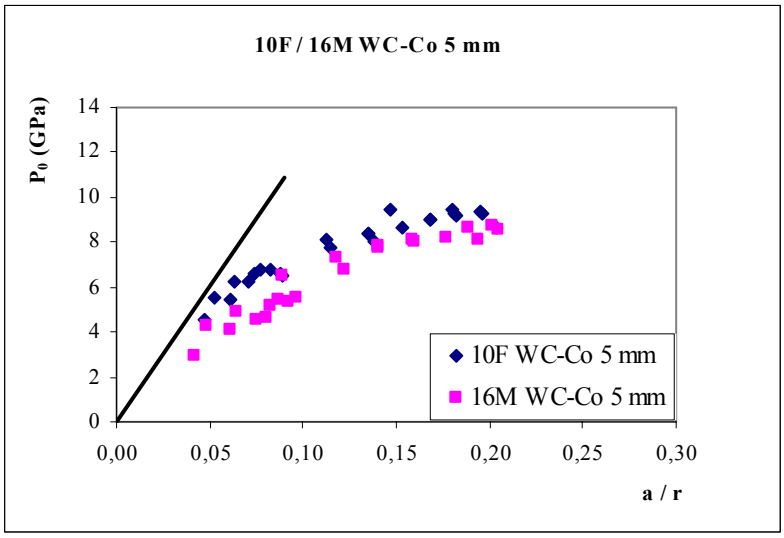

Figure 4.2*a*. Indentation stress-strain curves for 10F and 16M from Hertzian contact test for 5 mm WC-Ni indenter. Inclined solid line through origin is Hertzian elastic limit for 10F.

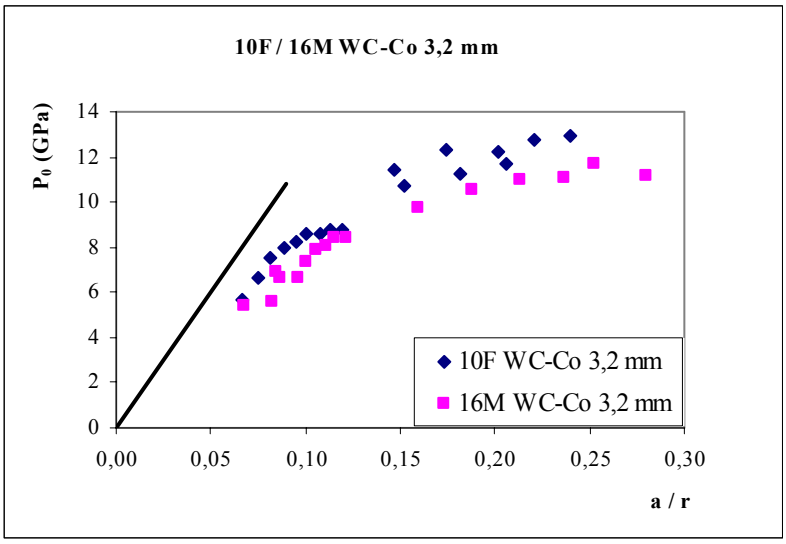

Figure 4.2*b*. Indentation stress-strain curves for 10F and 16M from Hertzian contact test for 3.2 mm WC-Ni indenter. Inclined solid line through origin is Hertzian elastic limit for 10F.

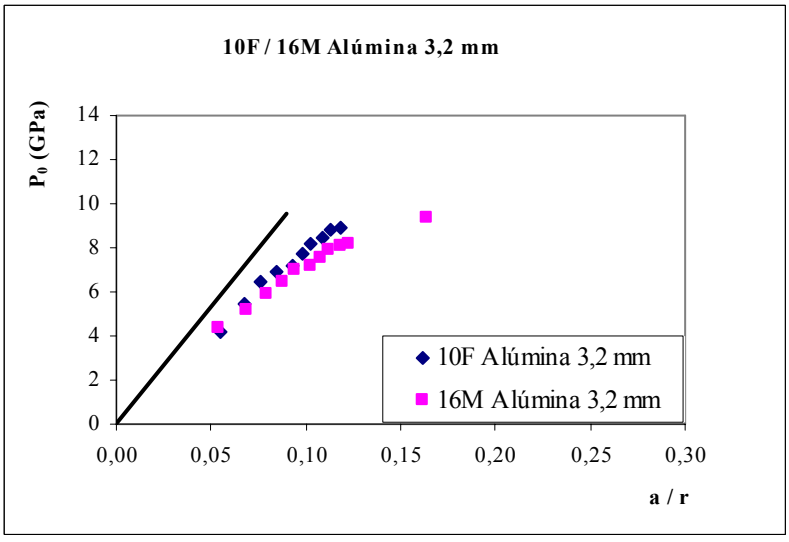

Figure 4.2*c*. Indentation stress-strain curves for 10F and 16M from Hertzian contact test for 3.2 mm alumina indenter. Inclined solid line through origin is Hertzian elastic limit for 10F.

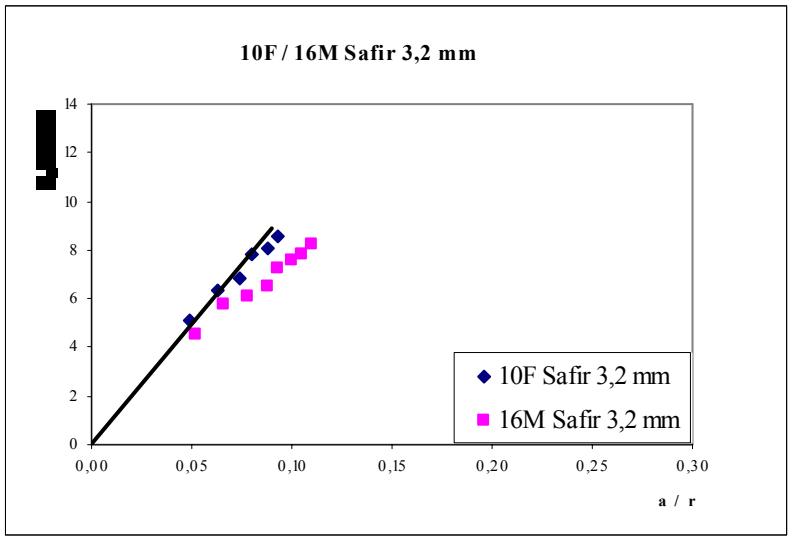

Figure 4.2*d*. Indentation stress-strain curves for 10F and 16M from Hertzian contact test for 3.2 mm sapphire indenter. Inclined solid line through origin is Hertzian elastic limit for 10F.

As it is clearly seen from table 4.2 and from the respective diagrams the theoretic values are higher in all the cases, perhaps except for sapphire indenter, than those obtained from experiments. There might be two explanations to this behaviour. First, it can be due to some systematic error made in measuring the contact radii, although all efforts were made to be as accurate and consistent as possible. The contact radii were measured plenty of times and in most cases there was no uncertainty that the correct value was obtained. In some cases it was more difficult to determine the exact radius due to poor contrast between the indentation print and the surrounding area. Although some indentations were repeated, the mark left in gold coating was not necessarily very clear; as it can be seen in figure 4.1*b*.

The second reason may be that there was some quasi-plastic deformation both at the indenter as well as at the studied materials even within the elastic regime. The deformation response scenario for the harder 10F material is shown in figure 4.3 where cross sectional views of bonded specimens clearly show the development of quasi-plastic damage. The loads used were: figure *a*) 300 N, *b*) 400 N, *c*) 700 N and *d*) 800 N, and indentations were made with WC-Ni 3.2 mm sphere. The arrows mark the limit of quasi plasticity.

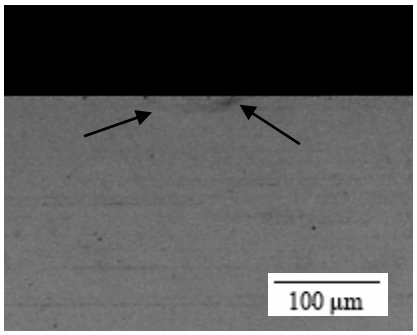

Figure 4.3*a*

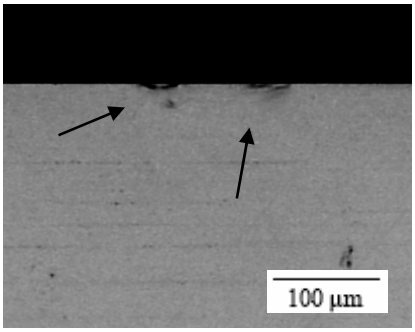

Figure 4.3*b*

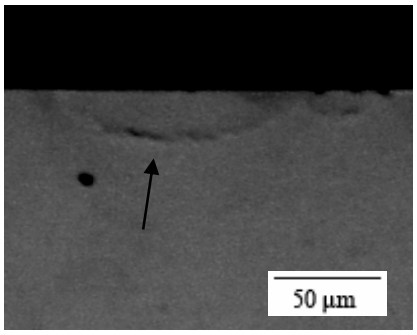

Figure 4.3*c*

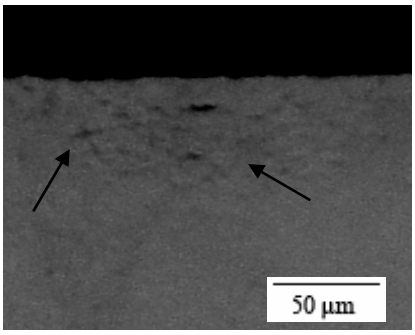

Figure 4.3*d*

Figures 4.3 showing the development of quasi-plastic deformation in 10F.

An examination of figures 4.2 shows that the experimental values for slopes presented in table 4.2 are highly uncertain, particularly for the WC-Ni indenters. It all depends when it is determined that there no longer is any straight line, which in this case is very difficult because there seems to be, apart from the very first points in figure 4.2*b* for 3.2 mm WC-Ni indenter, a clear deviation from this line along the whole curve. When the 5 mm indenter was used this deviation is even more evident, figure 4.2*a*, although the size of the indenter should not play any role here [6]. For alumina and sapphire indenters it is difficult to state how the curve would have continued if it had been possible to make indentations with higher loads. Nevertheless the very last points in these curves, figures 4.2*c* and *d*, appear not to be in line with the points before them.

The fact that the there is no linear relation between stress and strain implies that the material response is quasi-plastic in the range of the loads used during the experiments. This

conclusion is confirmed by the examination of figure 4.3*a*, which shows that there was quasi-plastic deformation already by the lowest load used when indenting the bonded specimen, i.e. 300 N. Also the fact that experimental values for slopes, table 4.2 and figure 4.4, are very similar for all indenters used, contradict the assumption that there would have some systematic error in measuring the contact radii, this because for sapphire indenter the contact area were clearly visible in all cases, as in figure 4.1*a*. The large deviation of 5 mm WC-Ni indenter in figure 4.4 from other indenters could be explained by the fact that it was noticeable deformed when indenting with higher loads. For 3.2 mm WC-Ni indenter the deformation was not that clear, although it was of same material.

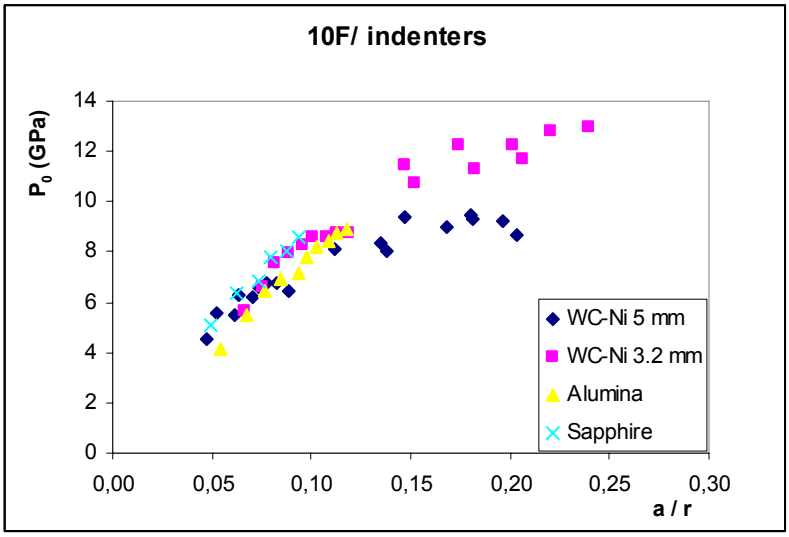

Figure 4.4. Comparison of indenters.

As there was quasi-plastic deformation in the whole range of loads used during this project, it can be said that the relation for purely elastic contacts from Hertzian theory, eq 4.1 cannot be used for assessing precise values in the indenter material system here studied.

On indenting brittle materials with spherical indenters a typical cone crack is often formed, called Hertzian cone crack [2], see figure 2.1. From the materials used in this project the 10F was more brittle than 16M, table 3.1. Hardness and toughness are two competing properties as it is well-known fact in material science. Considering this circumstance, if any hardmetal grade would have exhibited some downward propagating cone cracks it would have been 10F.

Figures 4.5 show the surface and section views of specimens when the surface ring cracks were formed in 10F. In the figures 4.5*a* and *b* with indentation load of 1000 N it is seen that although the surface cracks are wholly developed, at least in this half-block, the downward propagating cone crack is totally absent. In the figures 4.5*c* and *d* where the indentation was made with load 3000 N, there are more surface ring cracks and they are more evident, nevertheless the cone crack is hardly seen. There are some very small traces of cracks in the left of the figure, marked by an arrow.

The reason why the cracks formed on surface did not propagated downwards is that the volume beneath the contact area is in compressive stress, which suppresses the initiated cone cracks [2,4], together with the relatively low but intrinsic tough-like character of the 10F grade.

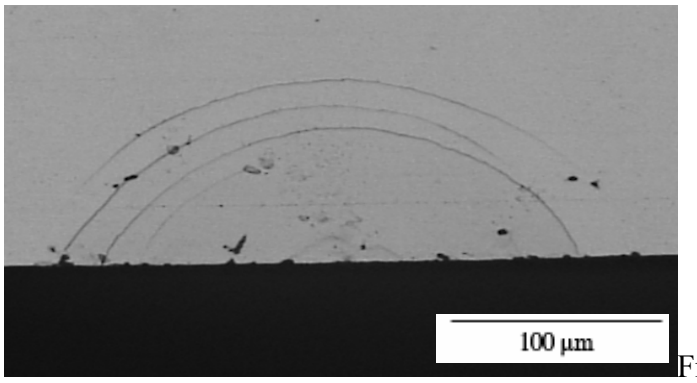

Figure 4.5*a*.

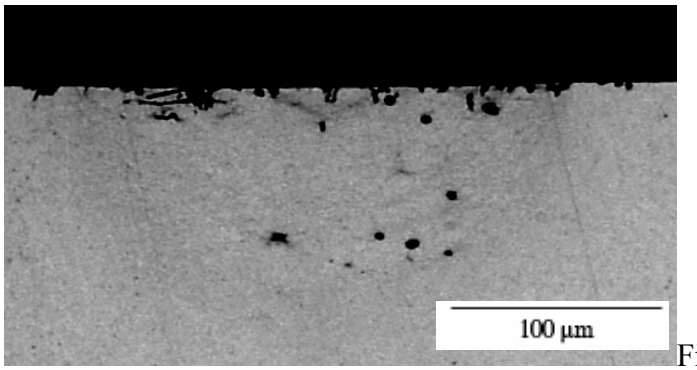

Figure 4.5*b*.

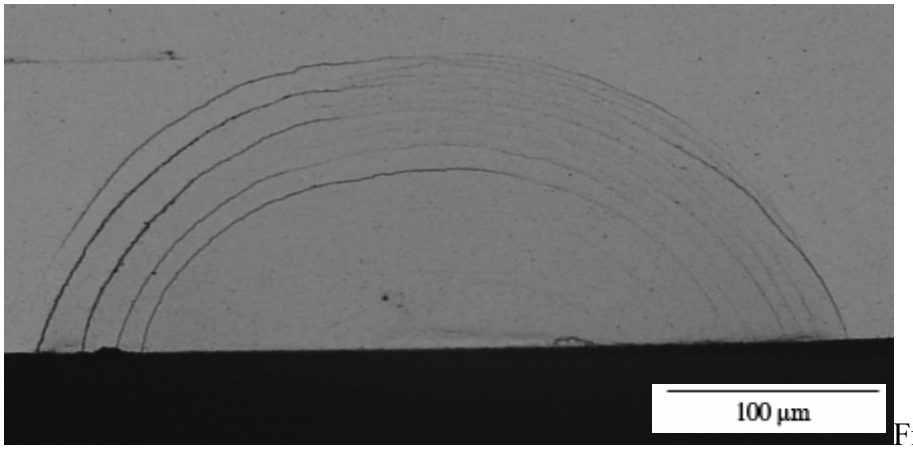

Figure 4.5*c*

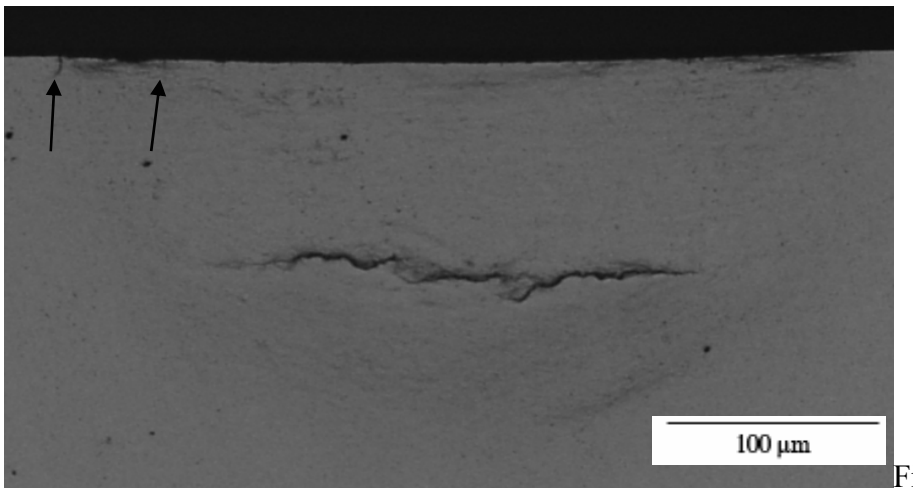

Figure 4.5*d*.

Figure 4.5 showing surface and section view of indentations of 10F with WC-Ni indenter, diameter 3.2 mm. Load 1000 N, figures *a* and b and 3000 N figures *c* and *d.*

4.1.2 Indentation of 16M

As mentioned earlier, when indenting 16M, both WC-Ni spheres endured the highest loads used 7000 N, but neither the surface ring cracks nor cone cracks showed out. Figures 4.6*a* and 4.6*b* indicate surface views of bar specimens after indenting with 5 mm and 3.2 mm spheres and with load 7000 N. Figures 4.7*a* and 4.7*b* show half surface and section views of bonded specimen for 3.2 mm sphere indentation and for load 3000 N.

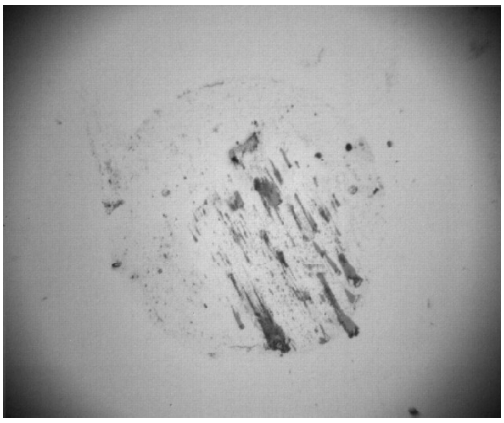

Figure 4.6*a*

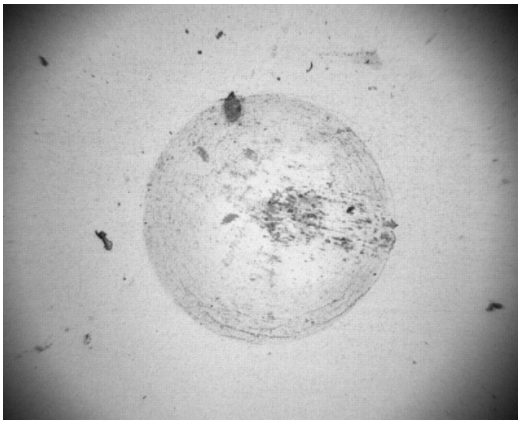

Figure 4.6*b*

Figure 4.6 showing the indentation of bar specimens of 16M with *a*) 5 mm and *b*) 3.2 mm spheres, load 7000 N.

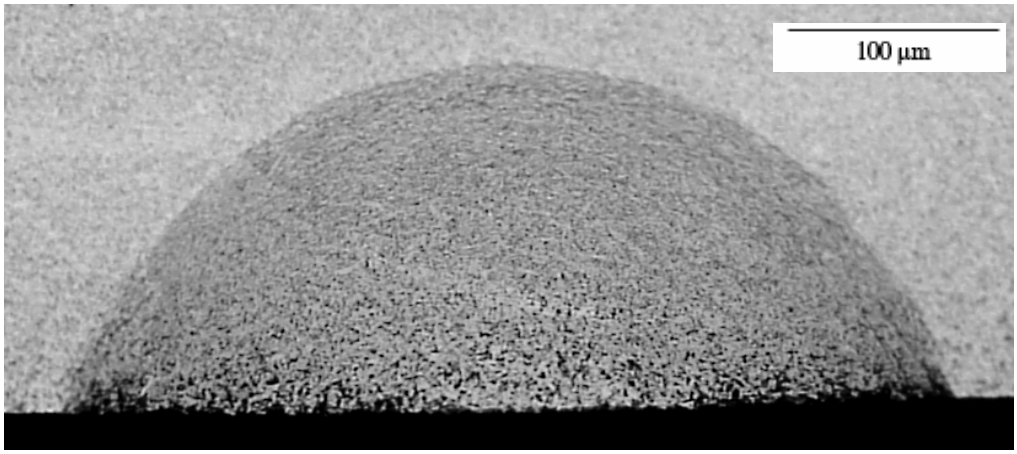

Figure 4.7*a*

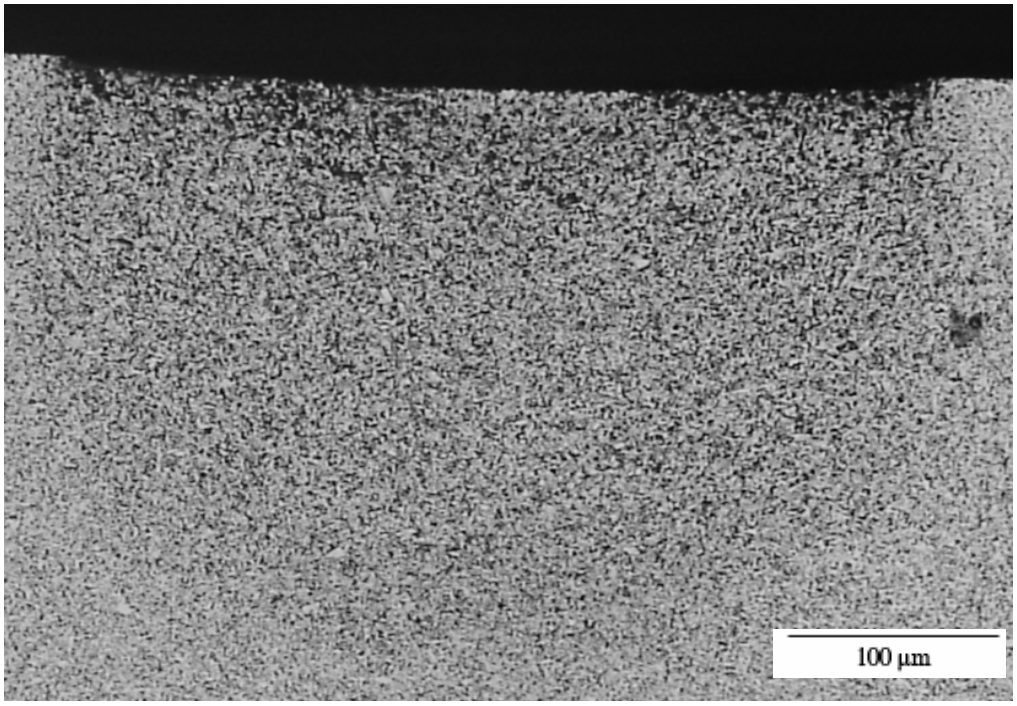

Figure 4.7*b*

Figure 4.7 showing the surface view of bonded specimen, figure 4.7*a*, and the section view, figure 4.7*b*. The load used here was 3000 N, which was the highest load used for bonded specimens.

Figures 4.8 *a*, *b* and *c* show the development of the quasi plasticity in 16M. The loads here are: *a*) 400 N, *b*) 700 N and *c*) 800 N Compared to corresponding figures for 10F it can be said, that for the load 400 N the quasi-plastic deformation is more noticeable in the case of 10F, which is somewhat surprising. For the loads 700 and 800 N there was no big difference.

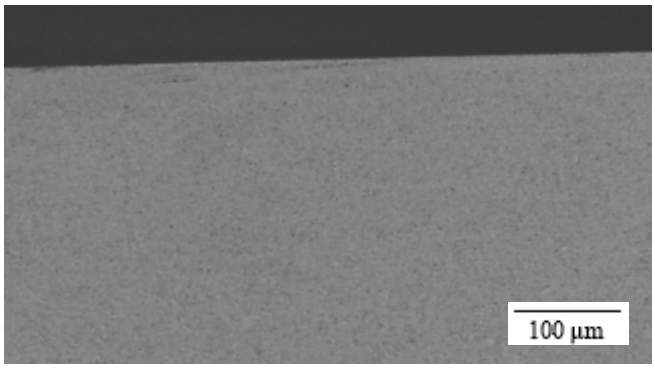

Figure 4.8*a*.

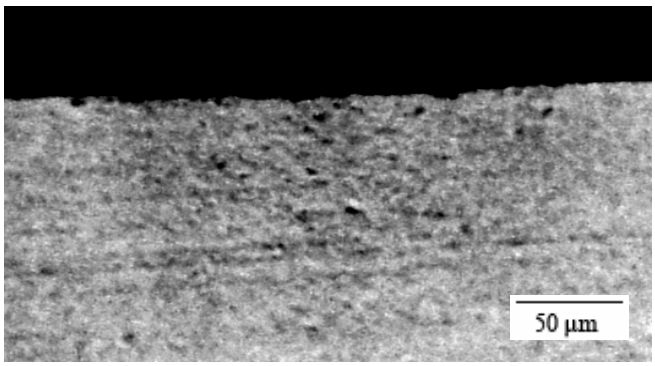

Figure 4.8*b*.

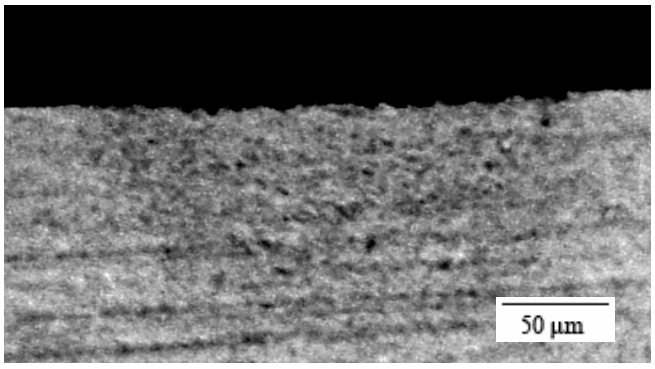

Figure 4.8c

Figures 4.8 showing the development of quasi-plastic zone in 16M.

When it comes to curves for 16M the first observation which should be pointed out is that the strain in all cases is larger for the grade 16M than for the grade 10F. This indicates a more significant quasi-plastic deformation in 16M, although this was not at all obvious when the figures above were compared. That the grade 16M would be more susceptible for quasi-plastic deformation than 10F was indeed expected due to material parameters mentioned earlier: higher binder volume percent and larger grain size.

Although the quasi-plastic deformation in all cases is more significant for 16M than for 10F, it is seen from figures 4.2*a*, *b*, *c* and *d* that the ratio between them is more or less constant. On the other hand for alumina and sapphire indenters it seems that deformation increases more rapidly for 16M, figures 4.2*c* and *d*. But here one have to keep in mind that these indenters broke at relatively low loads and consequently the number of indentations made is not high enough to make any reliable conclusions.

4.2 The scratch test

The scratch test conducted during the project gave similar results as the indentation test, that is, the 10F was harder and more brittle than 16M, and there were cracks seen on the scratch surface. The 16M did not show any cracks in this test neither. On the other hand scratch test showed more clearly than Hertzian contact test the difference of deformation properties between these two materials. Figure 4.9 compares these two materials by means of curve deformation-scratch load. The deformation “h” is the width of the scratch path and can be considered as a parameter for material removed during the test. It is clearly seen that deformation was larger for 16M by all applied loads demonstrating its softness in comparison with 10F. Although this was not really a wear test there might be an indication that 16M is more susceptible for wear than 10F. If that is true the reason may be coalescence of micro-cracks in quasi-plastic zone which were described in section 2 [8, 9].

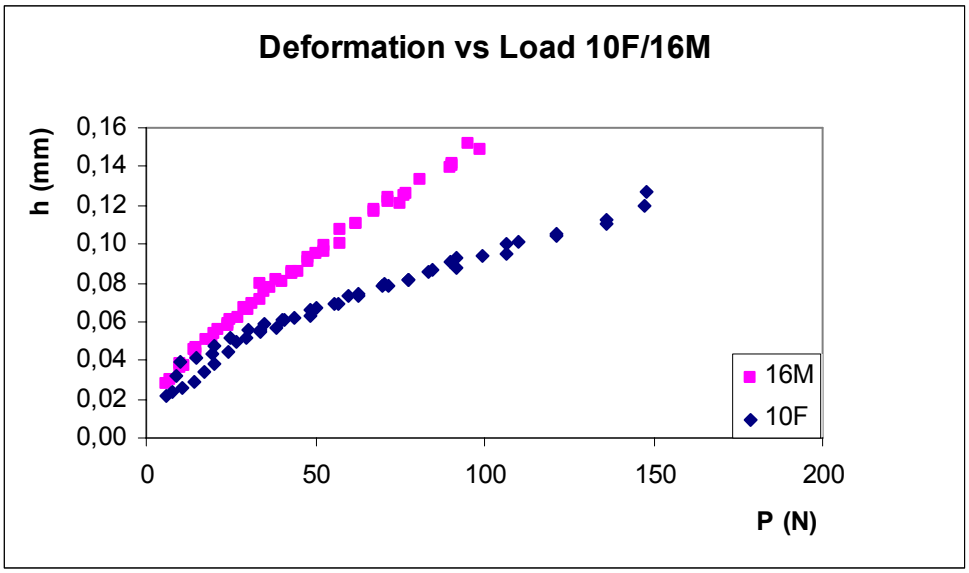

Figure 4.9. Comparison of 10F and 16M by means of curve deformation vs scratch load.

Figures 4.10 and 4.11 here below show the variation of acoustic emission and tangential frictional force as a function of normal scratch load. For both grades the frictional force is more or less constant, although for 10F there are some small tips in end of the scratch path and for the 16M it seems even to be slightly decreasing in spite of the fact that load increases constantly. This indicates that frictional coefficient for both grades decreases as well. There is not even fluctuation which would indicate that the material is chipping of, although the chipping is seen in figures later on in this rapport. One reason for the absence of the fluctuation could be that the chipping began so softly in 10F and became abrupt as the load increased. In the case of 16M, as it was not as hard as 10F, the chipping seems to have been soft along the whole scratch path. According to Lee et al. the smoothness of scratch groove indicates a plastic process [10]. When it comes to acoustical emission curve it increases linearly with load, although for 10F there is a slight rise at load 80 N. In figures 4.10 and 4.11 the unit for acoustical emission curve is arbitrary.

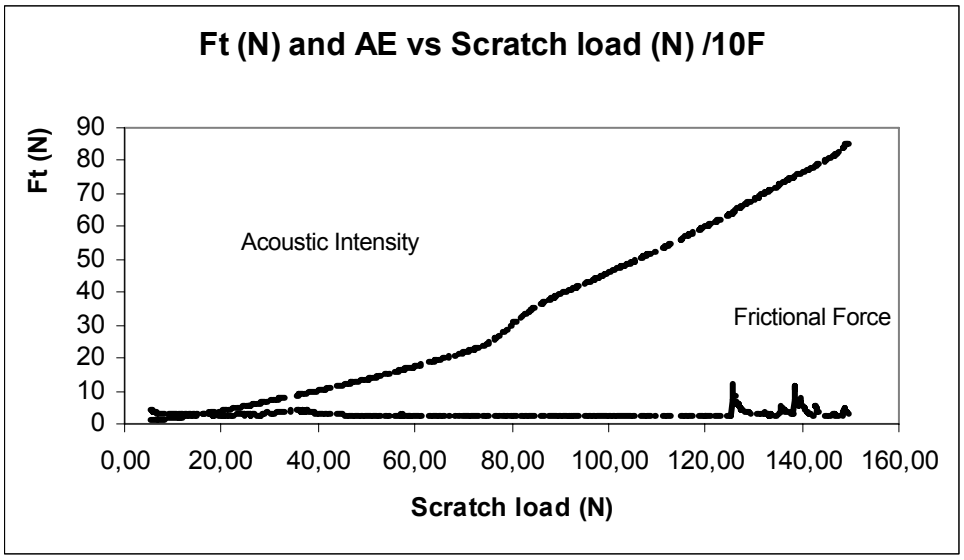

Figure 4.10. Acoustic signal intensity and tangential frictional force as a function of scratch load for 10F.

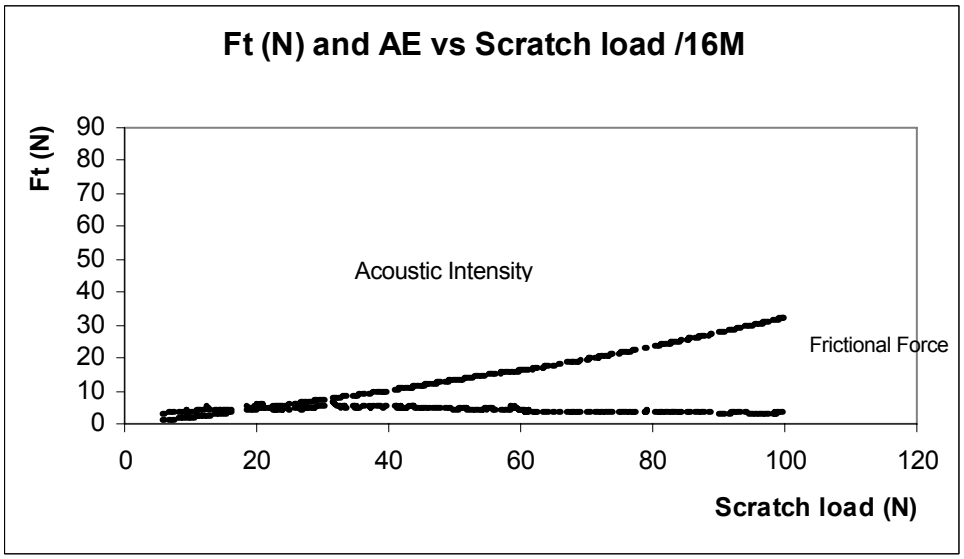

Figure 4.11. Acoustic signal intensity and tangential frictional force as a function of scratch load for 16F.

According to Sherman and Brandon crack damage in a scratch test approximates that of a Hertzian crack, and results from the tensile stress generated near the trailing edge of the contact. Cracks are formed when the external load exceeds a critical value. The trace of the scratch contains a set of cracks whose density is a function of the load, the surface conditions

and the indenter velocity [7]. To see if this is in accordance with results obtained during this project a comparison can be made. Figures 4.12*a* and *b* are from constant load test with sliding speed of 8.28 mm/min, the loads were 90 N and 110 N. The figure 4.12*c* is from progressive test, that is, when the load was increased constantly, with sliding distance of 2 mm and sliding speed 1.66 mm/min. The point where the load was 111.18 N is marked by an arrow. Although the cracks seem to be more evident for load 110 N than for load 90 N in constant load test or for load 111.18 N in progressive test, the density of them is more or less the same.

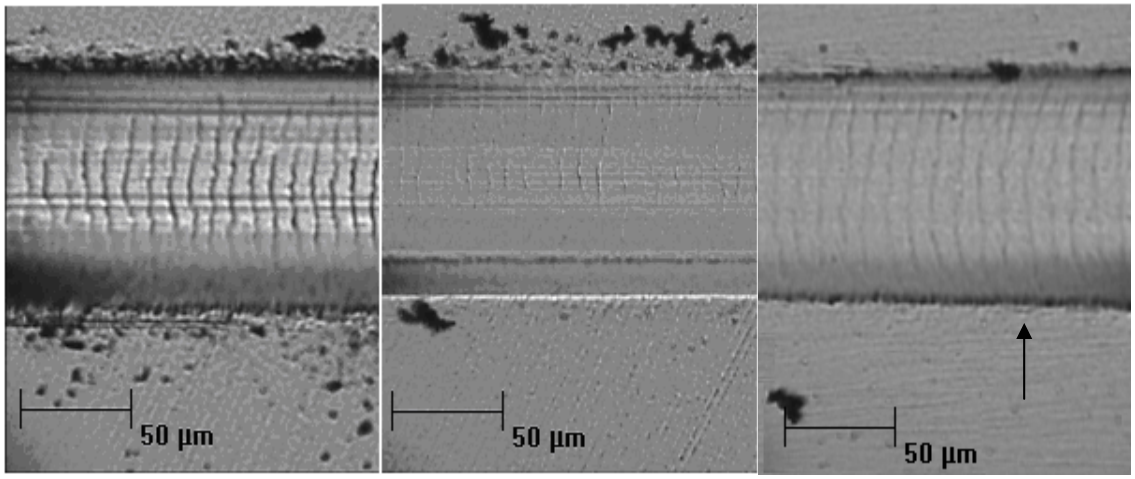

Figure 4.12 a) Figure 4.12 b) Figure 4.12 c)

Figures 4.12 showing the crack density dependency on applied load and sliding speed.

When it comes to other damage modes, the diagram below for 10F, figure 4.13, shows it clearly that test conditions had no considerable influence on test results. The comparison between progressive test and constant load test do not reveal any significant variation in stress-strain curves. No systematic difference was seen neither when it comes to magnitude of deformation nor to apparent critical loads, when the specimens were studied in optical microscopy. All this is said a bit reservation, namely when it comes to critical loads where the material began to chip of on borders of the scratch path there was a difference between the 2 mm and 10 mm test. For 10F the chipping began by load 111.18 N when the sliding distance

was 2 mm and by load 83.25 N when the sliding distance was 10 mm. For 16M the respective loads were 38.64 N for 2 mm test and 28.75 N for 10 mm test.

Certainly, in the case of 10F, when the strain is below 0.10, there is a large variation of stress values between the different test modes. The discrepancy is largest for the test where the sliding distance was 2 mm, i.e. when the increase of load per unit length was greatest. In the cases of sliding distance of 10 mm and constant load test only the first point in each case seems not to fit in the subsequent curve.

In the curve for 10F three different parts are clearly discerned. First an increasing part where the stress rises with strain, this part is also found in 2 mm test, even if it is shortest there. The second part is where the stress obtains its maximum and finally the third part, where the stress begins to decrease.

The first part, where the stress increases with strain, is probably due to homogenous deformation pointing out a strain hardening like behaviour. It can be seen that although there is a quasi-plastic deformation beneath the surface, figure 4.14*b*, no cracks are found on the surface, figure 4.14*a*. The crack propagating downwards in the figure 4.14*b* is probably caused when the indenter passed the interface between the two blocks. In the right side half-block there was no such crack. In the figure 4.14*c* it can be seen that the edge of the left half-block was much more suffered than the edge of the right one. The explanation to this behaviour is that, when the indenter slides, the material behind it is in tensile stress, while the material ahead it is in compressive stress. The load used here was constant and 50 N, which corresponds to stress 14 GPa. From figure 4.13 it can be seen that by this stress the curve for the constant load test begins to level off.

The cracks begin to appear on the surface by load 60 N, figure 4.15*a*. This load corresponds to stress 14.44 GPa., where the constant load curve obtain its maximum. The section view on figure 4.15*b* shows further subsurface quasi-plastic deformation compared to that in figure 4.14*b*, also the interface crack length in the left half-block is longer now.

The figures 4.16, 4.17 and 4.18 from constant load test show how the surface cracks and the subsurface quasi-plastic deformation become more and more evident with increasing load.

Above all, for the load 90 N, figure 4.17*a*, it is seen that the cracks are really obvious, here we recall also that in the figure 4.10 the curve for acoustic intensity rises a bit more steeply by load around and after 80 N. The cone crack typical for Hertzian contact test is totally absent for all loads. This was not really a surprise because it was not seen in a larger extent in test with spherical indenters neither.

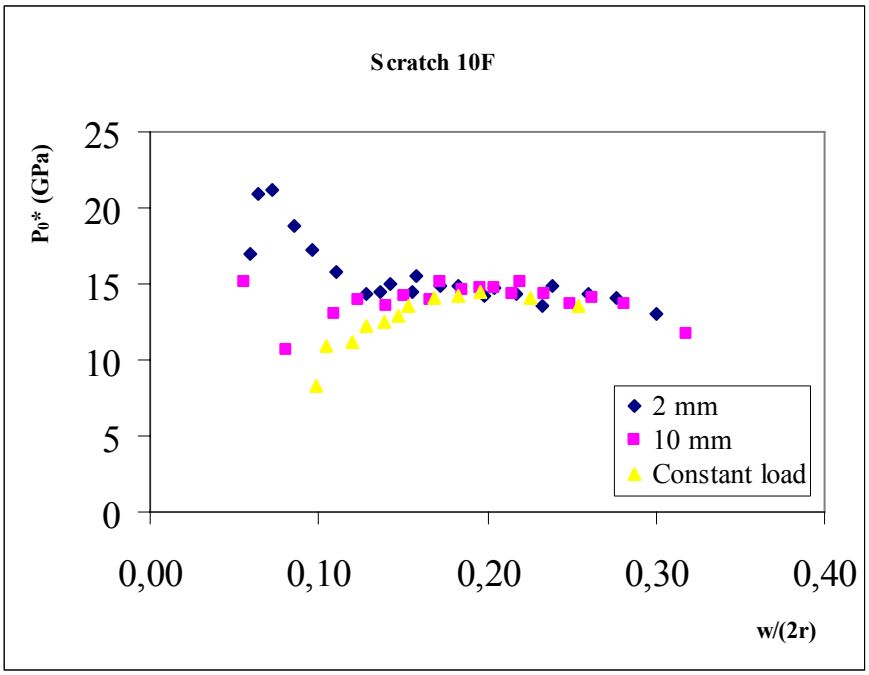

Figure 4.13. Scratch test stress-strain curve for 10F.

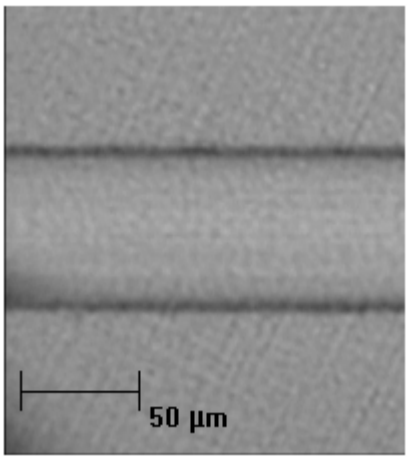

Figure 4.14*a*

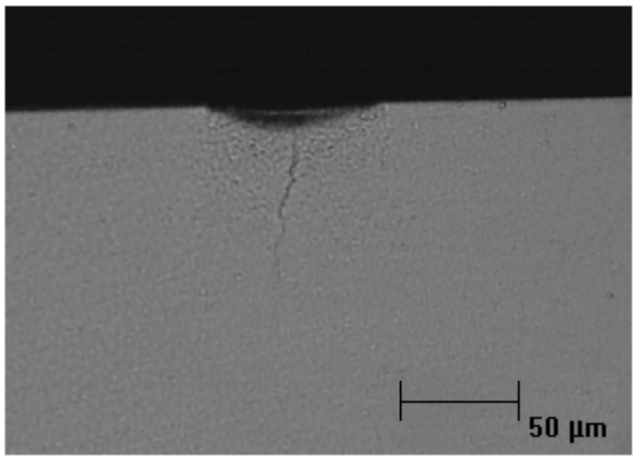

Figure 4.14*b*

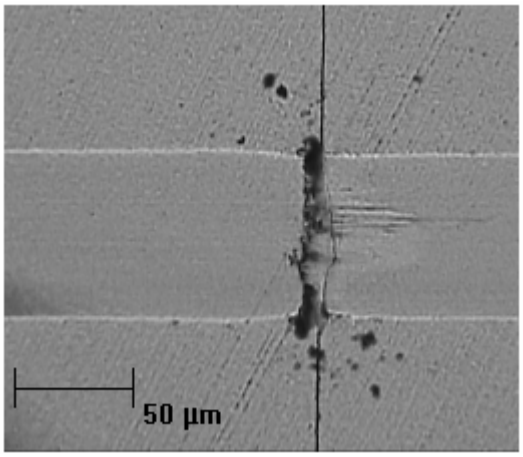

Figure 4.14*c*

Figure 4.14 for constant load test, 50 N. No cracks are seen on the surface in the figure *a*. The figure *b* is a section view from the left side half-block where a quasi-plastic deformation has taken place beneath the surface. The crack seen on the figure *b* is probably caused when the indenter passed the interface between the two blocks. In the right side half-block there was no such crack. The figure *c* shows the interface between the two blocks, it is clearly seen that the border of the left half-block is more broken than the border of right half-block. The indenter was moved from left to right in the figure.

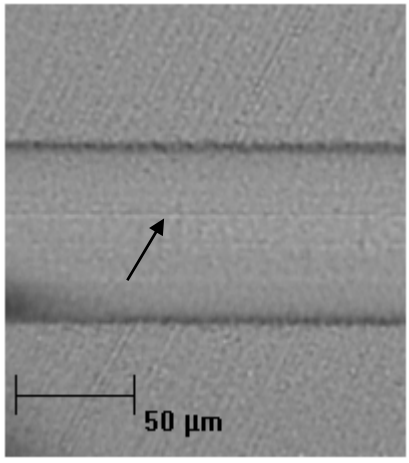

Figure 4.15*a*

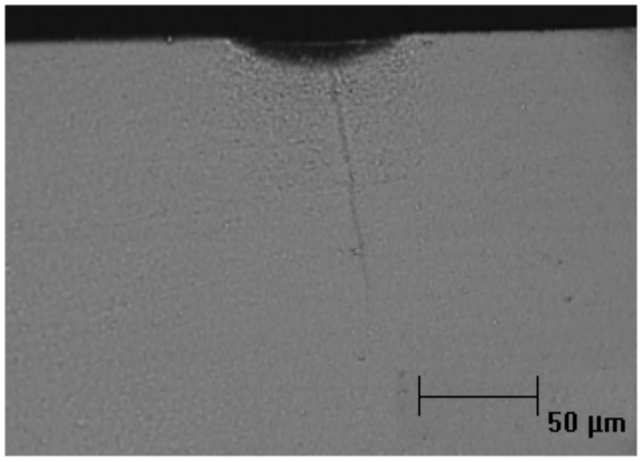

Figure 4.15*b*

Figure 4.15 showing the cracks that begin to appear on the surface by load 60 N, figure 4.15*a*. By this load the quasi-plastic deformation beneath the surface, figure 4.15*b* from the left half-block, is somewhat larger than with load 50 N, figure 4.14*b*, the interface crack is also longer now.

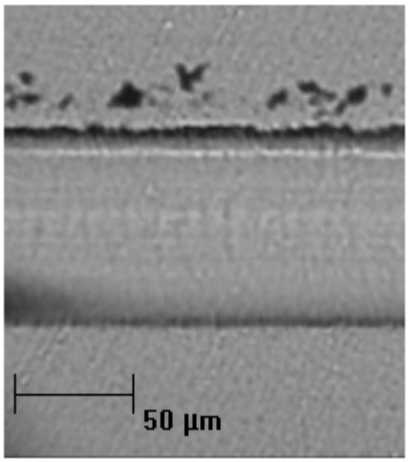

Figure 4.16*a*.

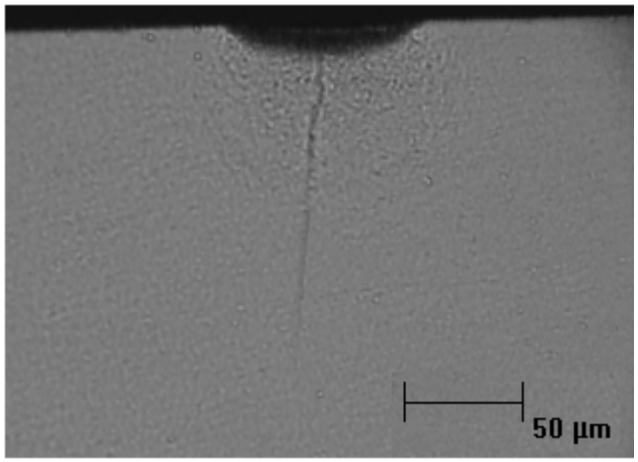

Figure 4.16*b*.

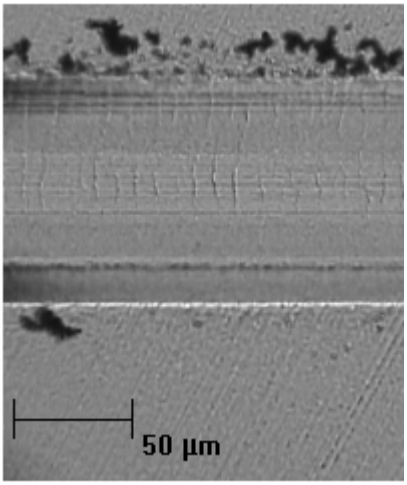

Figure 4.17*a*.

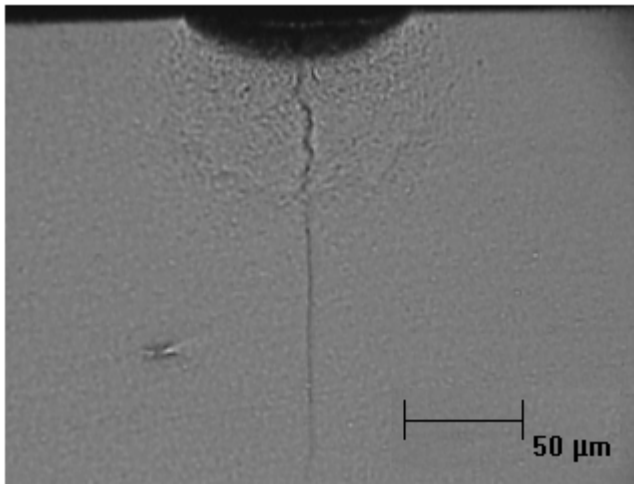

Figure 4.17*b*.

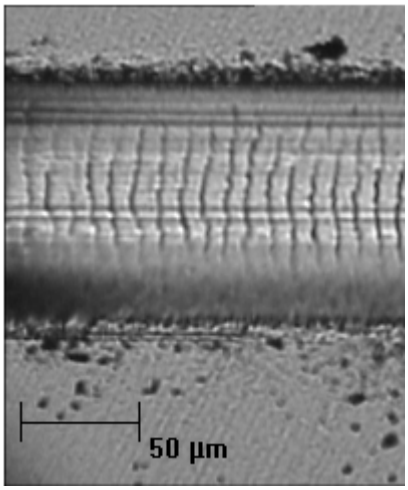

Figure 4.18*a*.

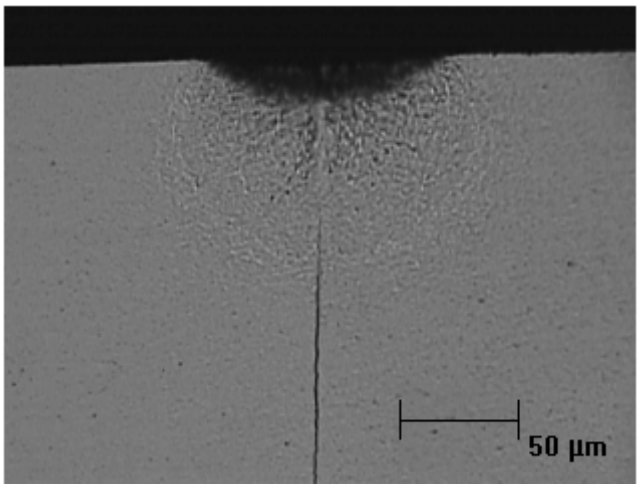

Figure 4.18*b*.

Figures 4.16, 4.17 and **4.18** here above show how the cracks and the subsurface quasi-plastic deformation become more and more evident with increasing load. 4.16) 70N, 4.17) 90 N and 4.18) 110 N.

The curves for 16 M, figure 4.19, show a linear relation between stress and strain for all type of test modes and almost in the whole range of loads used, from 10 to 90 N for constant load test and from 5 to 100 N for progressive test. By the strain of 0.10 there seems to be a plane part for 10 mm and constant load test. This might indicate that if the stresses had been lower, there would have been a same kind of increasing part in the beginning of the curves as in the case of 10 F.

In the scratched surface, not even by the highest load used, which was 90 N, there were not any cracks as those seen for 10 F, figure 4.20*a*. The interface crack was also absent, although the edge of the left side half-block was totally destroyed, figure 4.20*b*.

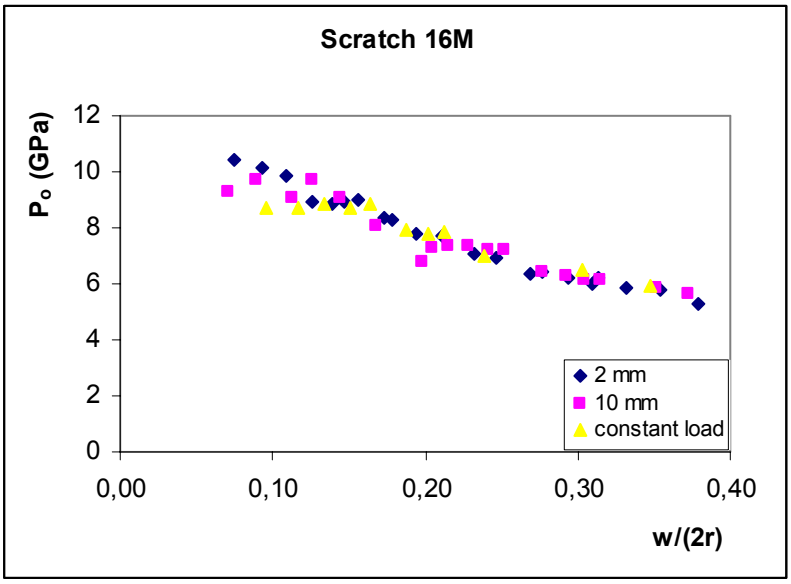

Figure 4.19. Scratch test stress-strain curve for 16F.

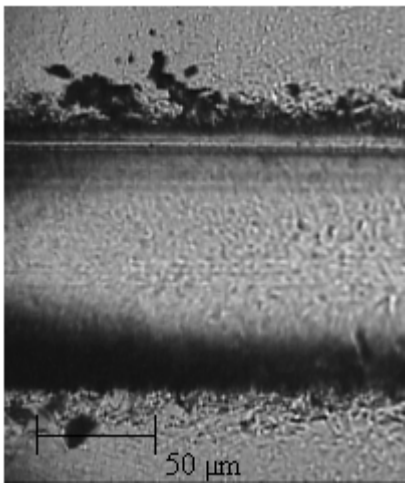

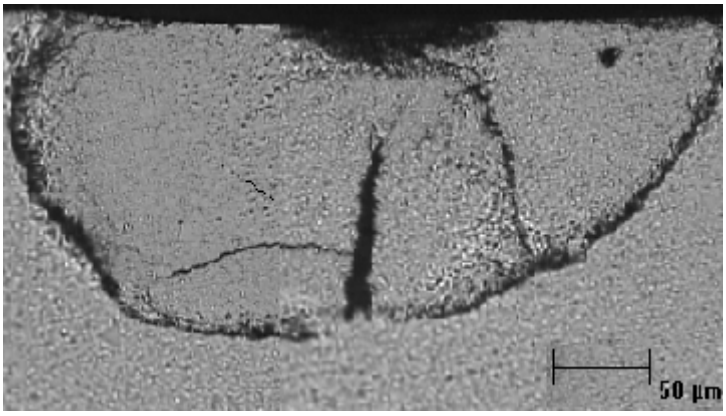

Figure 4.20*a* Figure 4.20*b*

Figure 4.20. 16M, scratch constant load, 90 N.

If we compare the curves for 10F and 16M, figure 4.21, it is seen that although the curve for 10F is above the curve for 16M, the slope for 10F seems to be more steeply falling at the end. This could be related to the presence of cracks in the surface of 10F, which grow and cause rapid degradation of material properties.

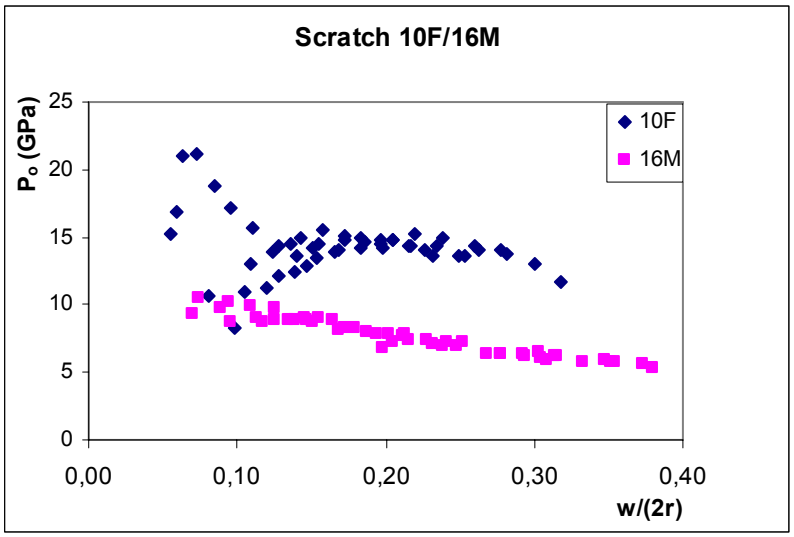

Figure 4.21. Comparison of the stress-strain curves for 10F and 16M.

Conclusions and Recommendations

Two different grades of cemented carbides, type WC-Co, have been studied: 10F and 16M. Deducing from material parameters the 16M was theoretically tougher (and more ductile) than 10F, because its volume content of metallic binder phase, cobalt, was twice that of 10F and the grain size of tungsten carbide phase was more than twice larger. Also the hardness of 16M was lower than for 10F.

The aim of this work was to evaluate the influence of the microstructure on the behaviour of these materials for different parameters of Hertzian contact and scratch test. The characterization of damage induced by contact with spherical indenters was made by optical microscopes. The examination with scanning electron microscope (SEM) did not bring any additional information about damage behaviour, this because studying the microstructure was not part of this work and for that reason the studies realised in SEM were not commented in text.

The assumption that 16M was more "plastic" than 10F was confirmed during the experiments. The first indication of this was received when indenting the bar specimens with different indenters. Except the 5 mm WC-Ni indenter all the other indenters broke at lower loads as the indentations were realised in 10F. This means that the plastic or quasi-plastic deformation was larger for 16M. Although the aim was to study whether there would be subsurface quasi-plastic deformation beneath the contact area or cracks, preferably Hertzian cone-cracks, the plastic deformation on the surface was also seen in both grades. The second proof of higher toughness of 16M was seen as the specimens were examined by microscope. In 10F there were clear surface cracks when the indentation loads exceeded 3000 N and 5000 N when indenting with spheres of diameter 3.2 mm and 5 mm, respectively, while in 16M no cracks were seen. On the other hand, the surface cracks in 10F did not propagate appreciable, which leads to conclusion that the catastrophic failure, which often follows when brittle materials suffer even a small damage, may not take place in this case.

The results from scratch test confirmed also the early assumption that 10F would be more brittle, however the 16M suffered more severe plastic deformation. This fact should be taken

into consideration when new applications of hardmetals are designed, such as bearings, for example.

In the light of results obtained, it can be said that although these materials in the first sight appears as relatively brittle materials, both of them showed some ductile behaviour when subjected to contact damage with spherical indenters. It may be stated that although the 10F was harder and more brittle than the 16M, it still exhibits an intrinsic "tough-like" character as compared to other brittle engineering ceramics such as alumina, silicon nitride or silicon carbide. Considering that 10F is about the hardest and most brittle hardmetal grade available on the market (under conventional technology) the findings here reported could be extrapolated to any WC-Co cemented carbide, fom a practical viewpoint.

For better understanding of damage behaviour of hardmetals a study in microstructural level should be carried out. In this work it was assumed that the damage mechanism of cemented carbides would resemble to that of ceramics', for example when it comes to subsurface quasi-plastic damage, and to validate or reject this assumption further studies are necessary. Also, a study of strength degradation after contact damage is important to conduct, since it seems that crack propagation is not as straightforward as in ceramics, recall the clearly manifested surface ring cracks in figure 2.2, which did not propagate downwards.

References

[1] UPADHYAYA G. S., *Cemented Tungsten Carbides: Production, Properties and Testing, Noyes Publications*, New Jersey, USA, 1998.

[2] LAWN B. R., *Indentation of ceramics with spheres: A century after Hertz*. Journal of the American Ceramic Society, 1998; 81,1887

[3] KOCER C, COLLINS R. E., *Angle of Hertzian Cone Cracks*, Journal of the American Ceramic Society, 1998; 81, 7.

[4] GUIBERTEAU F., PADTURE N. T., LAWN B. R., *Effect of Grain Size on Hertzian Contact Damage in Alumina*, Journal of the American Ceramic Society, 1994; 77,7.

[5] TORRES HERNÁNDEZ Y., *Comportamiento a fractura y fatiga de carburos cementados WC-Co*, Tesis doctoral, Departament de Ciencia dels Materials i Enginyeria Metal-lúrgica, Universitat Politècnica de Catalunya, 2002.

[6] LEE K. S., WUTTIPHAN S., LAWN B. R., *Role of microstructure in Hertzian contact damage in silicon nitride: 1, Mechanical characterization*, Journal of the AmericanCeramic Society, 1997; 80, 9.

[7] SHERMAN D, BRANDON D, *Mechanical Properties of Hard Materials and Their Relation to Microstructure*, Advanced Engineering Materials, Vol. 1, Issue3-4, (p. 161-181).

[8] RHEE Y. [et al], *Brittle Fracture versus Quasi Plasticity in Ceramics: A Simple Predictive Index*, Journal of the American Ceramic Society, 2001; 84, 3.

[9] LAWN B. R. [et al], *Making Ceramics «Ductile»* Science, 1994; 263.,5150.

[10] LEE S. K. [et al], *Scratch Damage in Zirconia Ceramics*, Journal of the American Ceramic Society, 2000; 83, 6.